Probabilistic volcanic mass flow hazard assessment using statistical surrogates of deterministic simulations

Stuart R. Mead[1], Jonathan Procter[1] and Mark Bebbington[1]

[1]Volcanic Risk Solutions, School of Agriculture and Environment, Massey University, Palmerston North, New Zealand.

Corresponding Author: Stuart Mead s.mead@massey.ac.nz

Authorship contribution statement

SM wrote the code, performed simulations and hazard assessment, and drafted the manuscript. JP contributed to development of manuscript, hazard simulations, editing and revision of the manuscript. MB contributed to statistical modelling, editing and revision of the manuscript.

Computer Code Availability

The open-source python code for the Probabilistic Surrogate, including sample data, is available from https://github.com/stuartmead/probablisticsurrogate. Modified Titan2D simulator source code used to create the source data is available in the Zenodo repository https://doi.org/10.5281/zeondo.153.993.

Highlights

- The computational expense of simulations limits probabilistic hazard assessment.
- Surrogate models can alleviate this through a fast approximation to simulations.
- Surrogate models provide a tractable solution to probabilistic hazard assessment.
- The methodology is demonstrated in an application to Taranaki volcano.

Abstract

Probabilistic volcanic hazard assessments require (1) an identification of the hazardous volcanic source; (2) estimation of the magnitude-frequency relationship for the volcanic

process; (3) quantification of the dependence of hazard intensity on magnitude and external conditions; and (4) estimation of hazard exceedance from the magnitude-frequency and hazard intensity relationship. For volcanic mass flows, quantification of the hazard intensity is typically undertaken through the use of computationally expensive mass flow simulators. However, this computational expense restricts the number of samples that can be used to produce a probabilistic assessment and limits the ability to rapidly update hazard assessments in response to (e.g.) changing source probabilities. We develop an alternate approach to defining hazard intensity through a surrogate model that provides a continuous estimate of simulation outputs at negligible computational expense, demonstrated through a probabilistic hazard assessment of dome collapse (block-and-ash) flows at Taranaki volcano, New Zealand. A Gaussian Process emulator trained on a database of simulations is used as the surrogate model of hazard intensity across the input space of possible dome collapse volumes and configurations, which is then sampled using a volume-frequency relationship of dome collapse flows. The demonstrated technique is a tractable solution to the problem of probabilistic volcanic hazard assessment, with the surrogates providing a good approximation of the simulator at very limited computational expense, and is generally applicable to volcanic hazard and geo-hazard assessments that are limited by the demands of numerical simulations.

Keywords

Probabilistic volcano hazard assessment; numerical modelling; surrogate modelling; emulation; pyroclastic flow

1 Introduction

Volcanic mass flows such as pyroclastic density currents, lahars, and debris avalanches are amongst the most hazardous volcanic phenomena generated by volcanic eruptions and unrest (Brown et al. 2017). Appropriate management and mitigation of risks to infrastructure and

population from volcanic activity therefore requires, as one component of risk, an estimation of the hazard posed by these phenomena (Brown et al. 2015; Magill and Blong 2005; Pareschi 2000). Hazard estimates that are quantitative and probabilistic are preferred for the purposes of decision support tools (e.g. cost/benefit analyses), measuring or ranking risks, and as an objective measure for (e.g.) asset or land-use planning (Marzocchi et al. 2012; Sandri et al. 2012). However, the specific hazard posed by each process can range from minimal to catastrophic depending on eruption magnitude, style, intensity, and environmental interactions (i.e. with the landscape for mass flows, with the atmosphere for tephra fall Hill et al. 2009). The large input space created by these eruption properties that can span several orders of magnitude, and many potential states of eruption style and environmental conditions form a critical obstacle to quantitative hazard assessment (Stirling et al. 2017; Stirling and Wilson 2002).

Here we refer to quantitative hazard assessments as those that provide a probabilistic estimate of intensity (e.g. height, velocity and/or pressure) for one or many volcanic phenomena (i.e. using common definitions of Connor et al. 2015; Marzocchi et al. 2012). In the framework of probabilistic volcanic hazard assessment (PVHA, Stirling et al. 2017; Stirling and Wilson 2002), quantification at any site of interest consists of four broad steps: (1) identification of volcanic sources that may generate hazardous phenomena; (2) estimation of magnitude-frequency relationship for the eruption source; (3) quantifying the dependence of hazard intensity on the eruption magnitude, site properties and environmental conditions; and (4) estimation of hazard exceedance from the magnitude-frequency and hazard intensity relationships. This follows a similar methodology to probabilistic seismic hazard assessments (PSHA), exploiting the relatively early development (Cornell 1968) and acceptance of seismic hazard modelling (Hill et al. 2009; Stirling et al. 2017).

The most mathematically complex elements in the PVHA approach occur in steps 2 and 3 (Stirling et al. 2017), which do not have accepted or easily computable solutions. Regarding an eruption source model (step 2), data completeness uncertainties (Mead and Magill 2014; Wang and Bebbington 2012) and intervolcano variation (Bebbington 2014) affect frequency-magnitude relationships. These are further complicated by the range of eruption durations, style and transitions between styles (Bebbington and Jenkins 2019) that may affect hazard intensity. Baseline probabilities of when and how large an eruption may be estimated through data (Damaschke et al. 2018) or expert elicitation approaches (Bebbington et al. 2018), and can be used to calculate conditional probabilities for (e.g.) hazard occurrence, eruption intensity, size and style. Provided with an eruption source model, the most logical approach to calculate hazard exceedance is through cross-multiplication of the source probability distributions ('input') with a hazard intensity model (e.g. Bevilacqua et al. 2017).

Numerical or statistical models that simulate volcanic processes (e.g. through commonly used simulation packages Titan2D, VolcFlow, Fall3D, Tephra2) are most often used to generate a hazard intensity model, as they also consider the effect of relevant site properties (e.g. terrain between source and site) and environmental conditions (e.g. wind speed and direction for ash fall). Hazard assessments using this (or a similar) PVHA approach have mainly been applied to ashfall hazard with either a single source (Biass et al. 2016; Bonadonna et al. 2005; Hurst and Smith 2004) or a multi-source region (Hurst and Smith 2010; Jenkins et al. 2012; Magill and Blong 2005), using Monte Carlo methods to sample the input space for simulation parameters. This is often possible through limiting input variables to only a few dimensions. The dominance of probabilistic ashfall hazard assessments (Calder et al. 2015) is mainly due to the availability of simulators that are fast enough to be directly used in Monte Carlo analyses. However, when applied to more computationally expensive simulators such as the Titan2D suite for volcanic mass flows (Patra et al. 2005), Monte Carlo methods become infeasible

(Mahmood et al. 2015). Critically for volcanic hazards, input distributions may change throughout a volcanoes lifecycle, episode or eruption event (see Jenkins et al. 2007 for terminology). This may require updating and further simulations of the processes (Spiller et al. 2014).

Monte Carlo approaches that sample simulator inputs differ from PSHA, and the Stirling et al. (2017); Stirling and Wilson (2002) conceptual outlines of PVHA, where a functional approximation of hazard intensity is used. These functions are often linear transformations, producing a hazard surface that can be rapidly queried to estimate hazard intensity, and its uncertainty for the entire spectrum of untested (or 'unseen') inputs. A classic example of such mappings are ground motion prediction equations (GMPE's) in seismology, but similar mappings (Bebbington et al. 2008; Rhoades et al. 2002) have been developed for ashfall based on the geologic record. A critical obstacle is developing functional approximations for volcanic mass flows (e.g. pyroclastic flows, lahars, debris avalanches) where robust models are difficult to develop from the geologic record due to physical processes that mask the record and large variability in flow initiation and dynamics. A proposed solution to this problem (Bayarri et al. 2009; Rutarindwa et al. 2019; Spiller et al. 2014) is to use an emulator, a fast statistical surrogate to computationally expensive simulations (Kennedy and O'Hagan 2001; Rasmussen 2006; Sacks et al. 1989). In simple mathematical notation, where a computationally expensive simulator produces outputs y as a function of the input configuration x as $y = f(x)$, an emulator is a suitably fast and accurate approximation of $f(x)$ (i.e. $\sim f(x)$) that can be substituted to find y at unsimulated inputs.

In this study, we focus on the use of emulation as a functional approximation (i.e. step 3 of PVHA) for probabilistic hazard assessment of dome collapse volcanic mass flows. Emulation techniques have been applied to volcanic mass flow hazards (e.g. Bayarri et al. 2009; Dalbey et al. 2008; Gu et al. 2018; Mahmood et al. 2015; Rutarindwa et al. 2019; Spiller et al. 2014;

Stefanescu et al. 2012), but focus on emulation to identify a specific catastrophic threshold or spatially mapping hazard. This is a 'hazard-centred' approach that is largely incompatible with (volcanic) multi-hazard assessments that are typically 'location-centred', using the location to identify and define the range of hazard sources and intensities (Carpignano et al. 2009; Nadejda et al. 2016). Our method uses warped Gaussian processes (Snelson et al. 2004) to simplify elements of the previous approaches (e.g. needing sub-emulators Rutarindwa et al. 2019; Spiller et al. 2014) and provide a continuous estimate of hazard exceedance. Using a location-centred approach, we refine and develop a PVHA methodology for volcanic mass flows to provide probabilistic hazard forecasts that integrate statistical modelling of source parameters, emulation methods and numerical simulations. This is demonstrated in an application to (probabilistically) forecast dome collapse impacts from Taranaki Volcano, New Zealand.

2 Methods used in probabilistic hazard assessment

2.1 Overview

A conceptual overview of the probabilistic hazard assessment process is shown in Figure 1. At the location of interest, the (individual) hazard exceedance probability is determined by creating models of the hazard intensity and its dependence on magnitude, site properties and environmental conditions ('Intensity-magnitude model', Figure 1) and the hazard source (i.e. the occurrence probability of magnitude, properties and environmental conditions, 'Hazard source model' in Figure 1). The source model produces values in the input space according to their probability distribution, which are then used to sample the hazard intensity model and define the exceedance function. Hazard source models for mass flows require the definition of a frequency-volume relationship, which is often conditional on probabilities of an eruption and

specific eruptive phases, in addition to relationships for site properties (e.g. direction of flow for pyroclastic density currents, Wolpert et al. 2018).

The source model probability spaces are mostly real-valued and likely to change in response to volcanic activity, therefore a continuous and easily sampled (fast) intensity model is

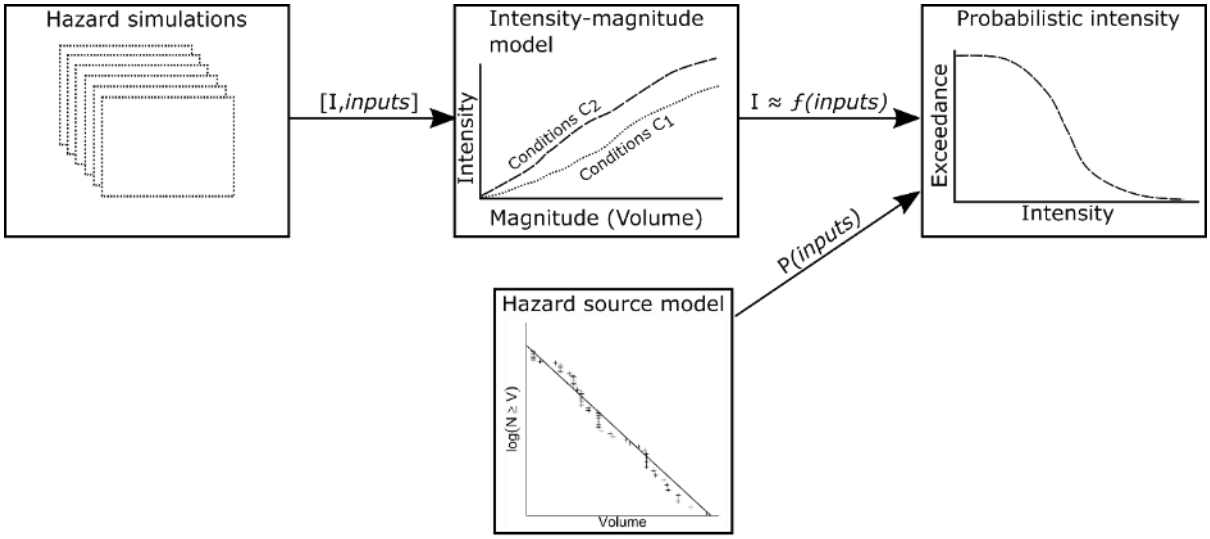

Figure 1. The probabilistic mass flow hazard assessment process.

preferred. However, mass flow hazard intensity cannot be easily modelled as a continuous function, so a statistical surrogate in the form of a Gaussian process emulator is used. A general framework for surrogate modelling using Gaussian process emulation is reasonably well established from earlier literature (Bayarri et al. 2009; Kennedy and O'Hagan 2001; Spiller et al. 2014). First, the hazard intensity at a set of predefined points within the input space (often in a space-filling design, Santner et al. 2003) is calculated using a computationally expensive, deterministic simulator (‘Hazard simulations’, Figure 1). Then, the simulation inputs and outputs are used as training data for the emulator to create a computationally efficient, continuous approximation of the simulator.

We use previously established source models and methods in this probabilistic hazard assessment, and therefore focus our methodology description on the simulation and emulation components of the surrogate modelling procedure to produce a hazard intensity model.

2.2 Volcanic mass flow simulation

Volcanic mass flows include dilute mixtures of particles in air (e.g. pyroclastic surges), dense, granular dominated flows (e.g. pyroclastic flows, block-and-ash flows) and, mixtures of granular material and water (lahars, debris avalanches, debris flows). The depth of these flows are typically much smaller than their large geographical extent. Depth-averaged simulation approaches which reduce computational complexity through a shallow-layer approximation are therefore well suited and frequently applied to the prediction of volcanic mass flow hazards (e.g. Aguilera et al. 2004; Bayarri et al. 2009; Charbonnier and Gertisser 2009; Kelfoun et al. 2017; Mead and Magill 2017; Patra et al. 2005; Pitman et al. 2003; Procter et al. 2010). The depth averaged system of equations in Cartesian coordinates can be expressed in terms of the height and momentum vector **U**, directional (x, y) flux vectors **F**, **G** and source (driving forces) vector **S** as:

$$\frac{\partial \mathbf{U}}{\partial t} + \frac{\partial \mathbf{F}}{\partial x} + \frac{\partial \mathbf{G}}{\partial y} = \mathbf{S} \quad (1)$$

We use a Mohr-Coulomb rheological model (Pitman et al. 2003) implemented in the Titan2D platform (Patra et al. 2005; Sheridan et al. 2005) for this application. The Mohr-Coulomb model for granular mass flows requires the following user specified inputs:

1. the terrain,
2. the initial volume, and its spatial distribution,
3. an internal friction angle φ, and
4. a basal friction angle, ϕ.

Previous studies have shown simulation results to be relatively insensitive to reasonable, mid-range values of internal friction angle (Procter et al. 2010; Sheridan et al. 2005), and the mobility of volcanic flows (expressed as $\tan(\phi)$) is relatable to the flow volume (Pudasaini and Miller 2013). The terrain input is commonly regarded as a fixed input for simplicity,

however is often subject to considerable uncertainty (Hawker et al. 2018; Stefanescu et al. 2012), and may change throughout a volcanic crisis. With terrain and friction angles fixed or having a fixed relationship, the input space of the simulator (χ) therefore consists of the variables needed to define the initial volume and its spatial distribution (location and shape). These inputs can be most conveniently and efficiently parameterised as an ellipsoid with constant aspect ratios (e.g. Procter et al. 2010) requiring the definition of four inputs: an initial volume (v), location (North and East coordinates; N, E) and orientation (azimuth, θ) of the elliptical pile.

While the application described here uses and makes simplifications on the basis of the Mohr-Coulomb depth-averaged approximation in Titan2D, the emulation procedure (described in following section) treats the simulator as a 'black box' consisting only of inputs and outputs. As a result, our framework is not restricted to the simplifications specifically mentioned here. Alternative simulators and rheological models for depth averaged systems of equations (e.g. Iverson and George 2014; Kelfoun 2017; Pudasaini 2012) may be substituted and additional inputs may be added with little methodological differences to the emulator.

2.2.1 Surrogate modelling of mass flow simulations

The simulator will produce a set of outputs (e.g. flow depth, dynamic pressure) for each simulation grid cell at any combination of the 4-dimensional input space ($\chi = [v, N, E, \theta]$), but at a great computational expense (e.g. ~12-24 hours on a 12 core processor). Our goal is to develop a fast and computationally cheap surrogate (emulator) for the simulator that provides an efficiently sampled (i.e. functional) representation of the input space. The emulation approach applied here borrows from the Bayarri et al. (2009); Gu et al. (2018); Spiller et al. (2014) Gaussian Process (GP) emulator methodology. The reader is referred to these publications for the full mathematical details, here we summarise the practical elements and key variations from the previous approaches important to this study.

Representing a scalar output of interest (y) from the simulator as $y = f(\mathrm{x})$; $(\mathrm{x} = [v, N, E, \theta])$, the GP emulator is a substitute for $f(\mathrm{x})$ as follows:

$$f(\mathrm{x}) \sim GP\big(\mu(\mathrm{x}), k(\mathrm{x}, \mathrm{x}')\big) \tag{2}$$

$$\therefore y \sim GP\big(\mu(\mathrm{x}), k(\mathrm{x}, \mathrm{x}')\big) \tag{3}$$

Where $\mu(\mathrm{x})$ is the mean (trend) with respect to x, and $k(\mathrm{x}, \mathrm{x}')$ is the covariance function across input pairs. The mean function $\mu(\mathrm{x})$ is often taken as zero or a fixed basis expansion for simplicity, as it simply normalises (to $\mu(\mathrm{x})$) the differences in x (Rasmussen 2006).

The covariance function (also called a kernel, Lloyd et al. 2014; Rasmussen 2006) defines the correlation structure between inputs (x, x') across the input dimensions, controlled by a set of free parameters (hyperparameters). A useful feature of kernels is that they can be combined across and within input dimensions as a sum or product of different kernels (e.g. $k(\mathrm{x}, \mathrm{x}') = k_1(\mathrm{x}, \mathrm{x}') + k_2(\mathrm{x}, \mathrm{x}')$). This compositional property is convenient for model selection and aids interpretability (Duvenaud et al. 2013), as covariance functions can be defined for each dimension individually (a conceptually simple task for domain experts) rather than *en masse*. For computer simulation outputs, smoothing kernels such as the squared exponential and Matérn kernels are most common (e.g. in Bayarri et al. 2009; Gu et al. 2018; Rutarindwa et al. 2019; Spiller et al. 2014). The primary free parameter in these smoothing functions is the lengthscale ℓ, a measure of the correlation distance between input values. In our simulations, expecting some degree of multi-scale variation as the pile volume and location changes, we choose a Matérn 3/2 kernel for the volume, North and East dimensions. In the orientation dimension, we expect smoother correlation and choose a periodic Matérn 5/2 kernel, with a period of π due to symmetry of the ellipse. Our covariance kernel is therefore:

$$k(\mathrm{x_i}, \mathrm{x_j}) = \prod k_{x=[v,N,E,\theta]}(\mathrm{x_i}, \mathrm{x_j}) \tag{4}$$

where

$$k_{x=[v,N,E]}(\mathrm{x_i}, \mathrm{x_j}) = \left(1 + \frac{\sqrt{3}r}{\ell}\right)\exp\left(-{\sqrt{3}r}/{\ell}\right), \qquad \mathrm{x} = [v, N, E] \tag{5}$$

$$k_{x=\theta}(\mathrm{x_i}, \mathrm{x_j}) = \left(1 + \frac{\sqrt{5}r}{\ell} + \frac{5r^2}{3\ell^2}\right)\exp\left(-{\sqrt{5}r}/{\ell}\right), \qquad \mathrm{x} = \theta \tag{6}$$

$$r = \left|\mathrm{x}_i - \mathrm{x}_j\right| \tag{7}$$

Inserting equations 4 to 5 into equation 3 defines a function parameterised with 4 unknown lengthscales and the mean function. Estimating the lengthscale hyperparameters using Maximum Likelihood Estimation (MLE) is often unstable (Gu et al. 2018; Spiller et al. 2014). This issue can be solved through specification of a prior (the 'reference prior', Berger et al. 2001) and finding the posterior mode (i.e. MAP estimate, Bayarri et al. 2009; Spiller et al. 2014). We use the ʻjointly robust priorʼ of Gu (2019), an easily computable objective prior with similar properties to the reference prior (Berger et al. 2001) that yields a proper posterior distribution.

Another difficulty encountered in GP emulation of mass flow simulations is the presence of zero values in our quantity of interest (e.g. flow height). At any location a reasonable distance from the source, a large portion of the simulation input space (of volume, ellipse location and orientation) will produce an output value of zero, abruptly changing to non-zero and then increasing monotonically with volume. Such an output is non-stationary, a property which causes difficulty when fitting the GP emulator (see e.g. Spiller et al. 2014). Solutions to this problem have been proposed and include partitioning (e.g. Treed-Gaussian Process, Gramacy and Lee 2008), input or output warping (Snelson et al. 2004; Snoek et al. 2014) and non-stationary covariance functions (Paciorek and Schervish 2004). For this task we found warping of the model output vector produced the most robust results. This approach, outlined in Snelson

et al. (2004), transforms the model outputs (y_m) by a series of hyperbolic tangent (*tanh*) steps with a linear trend outside the function bounds:

$$f(y_m; \{a, b, c\}) = y_m + \sum_{i=1}^{I} a_i \tanh\big(b_i(y_m + c_i)\big) \quad a_i, b_i \geq 0 \tag{8}$$

Where *a* scales the step size, *b* the steepness and *c* controlling step position for any number of *I* steps. We use a single step in this study as our output data is relatively simple (zero values, then monotonic increase), although any number of steps could be used.

Following Gu and Berger (2016), we add a noise term ('nugget') to equation 3 (i.e. approximate $y = f(x) + \epsilon$), as the basal friction input is masked from the emulator. The final emulator therefore contains 8 parameters (3 from equation 8, 4 lengthscales and the nugget), which was optimised using a SCG optimisation algorithm through the GPy package (GPy, 2012).

3 Emulation of dome collapse flows at Mt. Taranaki

3.1 Geologic setting and eruptive history of Mt. Taranaki, New Zealand

Mt. Taranaki (2518 m) is near-symmetrical andesitic stratovolcano with more than 170,000 years of geologic history (Alloway et al. 2005). The volcanic activity of Mt. Taranaki is cyclical, with large, unconfined debris avalanches initiated by destruction of former Taranaki edifices beginning the cycle (Zernack and Procter 2021). Regrowth of the Taranaki cone follows through smaller-scale activity, including small explosive eruptions, lava flows and dome growth. This activity can shift into larger scale explosive activity with large Plinian and sub-Plinian eruptions; block-and-ash flows; and the generation of long-runout, but confined mass flows (Zernack and Procter 2021).

Activity since the last debris avalanche (~7,000 years ago) is represented through a regrowth phase of 53 different eruption episodes identified in proximal deposits on Taranaki. These indicate complex eruption sequences associated with the generation of ashfall deposits and

small-scale pyroclastic density currents from eruption columns, longer-runout block-and-ash flows, and syn-eruptive or secondary lahars following valley and river channels in the Taranaki region (Torres-Orozco et al. 2016). The last 1000 years of activity (the Maero Eruptive Period, Neall 1979; Platz et al. 2007) is dominated by small eruptions (Volcanic Explosivity Index 3-4) with emplacement and collapse of lavas and smaller domes on the summit of Mt. Taranaki (Neall et al. 1986; Torres-Orozco et al. 2017; Zernack 2008).

A detailed account of pyroclastic flows during the Maero Eruptive Period is reported in Platz et al. (2007) who identified at least 10 separate flow events over the past 900 years. These flows affected two main sectors of Mt. Taranaki: the W-NW sector towards Stony (Hangatahua) River and the N-NE sector towards Ahukawakawa Swamp (Figure 2). This distribution of dome collapse pyroclastic flows is strongly influenced by the summit morphology (Lerner et al. 2019). Currently, the summit contains remnants of a lava dome (~1.5 x 10^6 m^3) within a 420 m diameter crater breached from the SW to NE ('The Chute', towards Stony River, Platz et al. 2007). This morphology directs most block-and-ash flows towards the NW sector of Egmont National Park; the past ~800 years of block-and-ash flows have almost exclusively impacted this sector (Procter et al. 2010). The hazard is assessed across three different locations (shown in Figure 2) to compare and quantitatively examine the effect of this morphology.

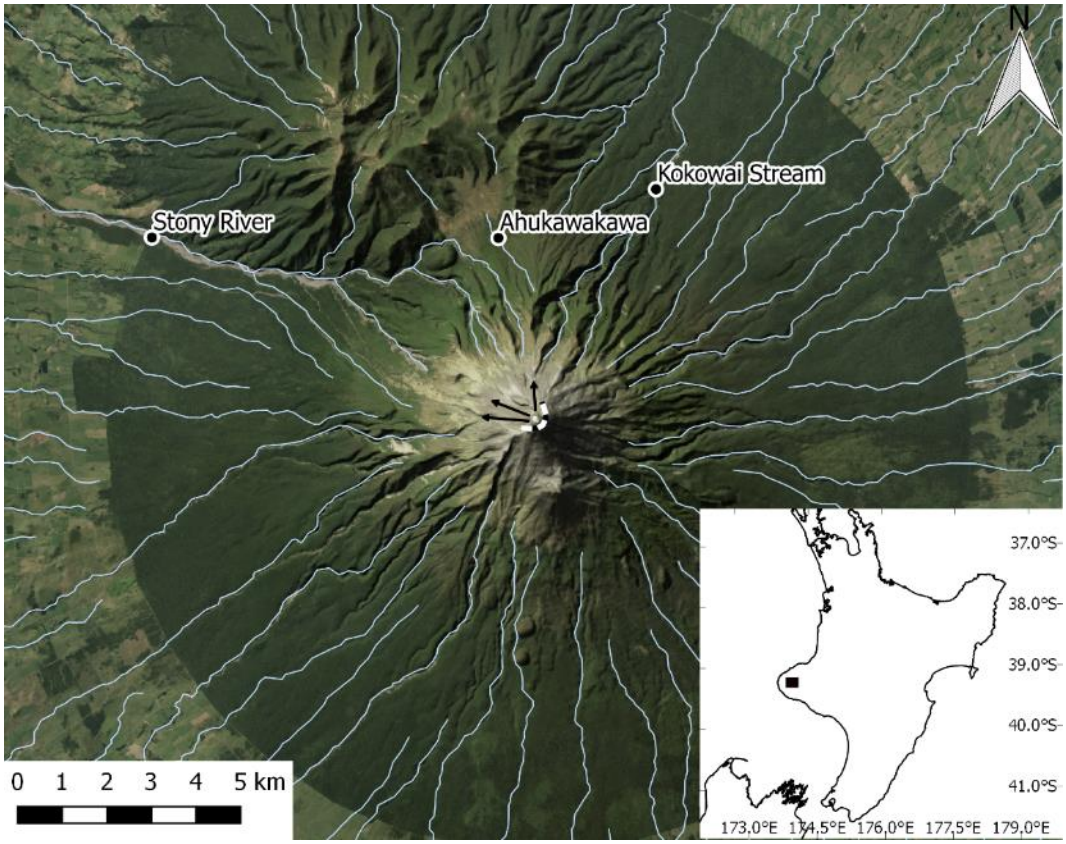

Figure 2. Taranaki volcano in Egmont National park with flow measurement points used in this study. Arrows show major flow paths for block-and-ash flows during the Maero eruptive period (Platz, 2007), dashed line shows crater rim.

3.2 Simulation of dome collapse pyroclastic flows

Dome collapse flows from the Taranaki summit appear to have lower energy in contrast to (e.g.) lateral blast triggered pyroclastic density currents, and dynamics are approximated well with a Mohr-Coulomb rheological model (Platz et al. 2007; Procter et al. 2021). Unit volumes for the Maero period come collapse flows range from 1-15 × 10^6 m^3, but likely represent a collection of smaller flows (Procter et al. 2010). A previous study of summit dome collapses (Procter et al. 2010) simulated flows with a volume of 10^6 m^3 using the Mohr-Coulomb model in Titan2D, which matched well to mapped deposits with similar volumes. Our simulation study introduces more variation to the summit dome configuration.

A half-ellipsoidal collapse shape was assumed with aspect ratios matching those of the previous dome (from Platz 2007) and volumes ranging from 10^5 to 10^7 m^3. The maximum volume corresponds to the presumed maximum dome volume possible in the summit crater, but is

larger than the maximum dome collapse flow volumes expected at Taranaki (Procter et al. 2010). We specify a larger volume in this case to expand the simulation input space beyond 'realistic' to ensure adequate support for the surrogate modelling and sampling (e.g. as in Rutarindwa et al. 2019). Similar 'expanded' input spaces are used to vary the planimetric centre and orientation of the dome, accounting for scenarios where a new dome is emplaced on the summit following an explosive eruption to clear the remnant dome (a possible scenario described in Ogburn et al. 2015). The centre of the collapsing ellipse from the summit vent varied in polar coordinates (0 to 210 m radius, 0 to 2π angle), transformed into planimetric (N, E) coordinates for input. The orientation of the ellipse major axis is also varied between 0 to 180° (current orientation ~117.5°). The internal friction coefficient, shown to have little effect on simulations (Procter et al. 2010; Sheridan et al. 2005), is set at 30° and basal friction is determined as a function of volume using the friction-volume relationship for volcanic mass flows (Pudasaini and Miller 2013). A total of 1024 input configurations (a set of $[v, N, E, \theta]$) were simulated, with inputs chosen in a space filling design (latin hypercube sampling). All simulations used a 25 m digital elevation model (Landcare Research NZ 2002).

The simulation output of interest (y from Equation 3) in this study is the maximum flow depth throughout the entire simulation. Results from all simulations are shown in Figure 3, aggregated to show the minimum volume required to exceed a threshold flow height of 1.0 m (typical heights for a catastrophic flow are between 0.25 and 1.0 m, Spiller et al. 2014). The simulations show most valleys within Egmont National Park are affected by dome-collapse flows in the range of dome configurations described, and that impact (as defined by the height threshold) increases with volume in a largely monotonic manner. Across the three locations in this study, flows need to exceed a critical volume (5.0×10^6 for Ahukawakawa and Stony River, 2.5×10^6 for Kokowai Stream) to cause impact above the threshold 1.0 m. However, the simplistic assessment in Figure 3 disregards the effect of location and orientation input

variables. This can be explored through the use of Gaussian Process emulator fitted to data for the three locations in Figure 2.

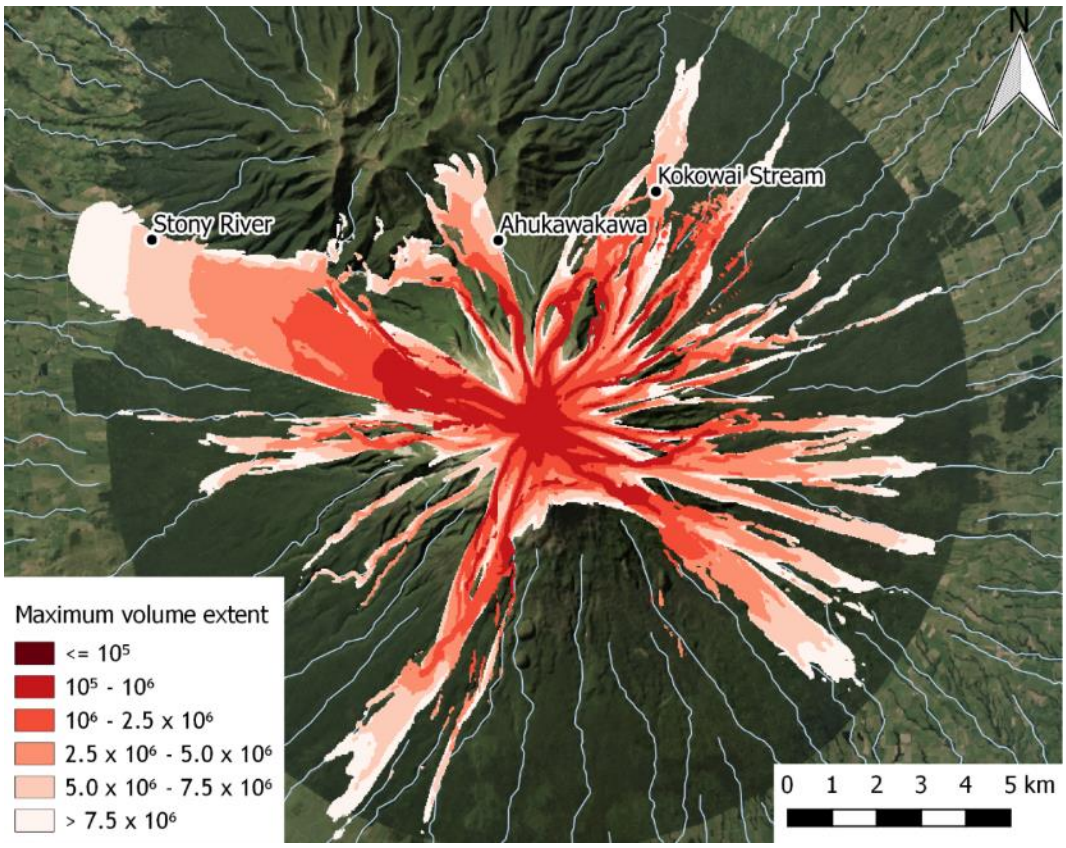

Figure 3. Map of minimum block-and-ash flow volume to exceed 1.0 m in flow depth for all simulations.

3.3 Emulator

Figure 4 shows leave-one-out cross-validation results (calculated using Vehtari et al. 2016) for the emulators fitted to each location of interest. The emulator mean is within 2 standard deviations of almost all (>90%) of the simulated values, although the errors (red in Figure 4) show some bias towards over-estimating at very low (simulated) height. Over-estimation is

preferred to underestimation in terms of risk, and uncertainties at very low heights are expected to have less of an effect on estimated hazard (examined in the following section).

The emulators can be used to examine 'slices' of the input space by providing a continuous

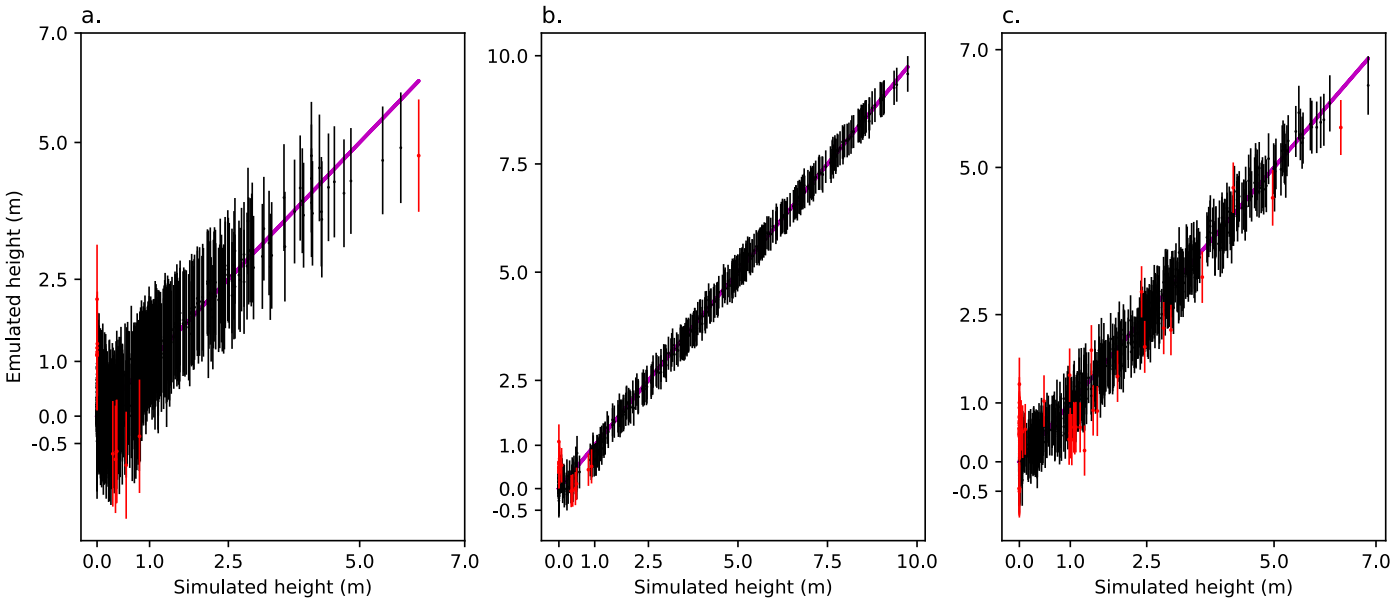

Figure 4. Leave-one-out cross-validation results for emulators fitted to simulation data at (a) Ahukawakawa, (b) Stony River, and (c) Kokowai Stream. Dots indicate the mean estimate, error lines are ±2 standard deviations of the mean, red points highlight estimates that are greater than 2 standard deviations from the simulated flow height. Magenta line indicates a perfect fit.

estimation across any dimension (or a combination of dimensions). Two examples of these are shown in Figure 5 and Figure 6. Figure 5 shows the emulator mean and 95% confidence interval for dome collapse flows with a location and orientation similar to the current dome and volume varying between 10^5 and 10^7 m^3. The prediction for Ahukawakawa (Figure 5a) indicates flow heights are expected to be less than 2.5 m in any volume scenario with the current dome configuration. The emulated flow height is much higher for Stony River, in agreement with the observations of a preferential flow direction in Platz et al. (2007). Emulated heights for

Kokowai Stream also indicate a critical volume (>2.5 × 10^6 m^3) is necessary to overcome topographic barriers and direct flow towards this location.

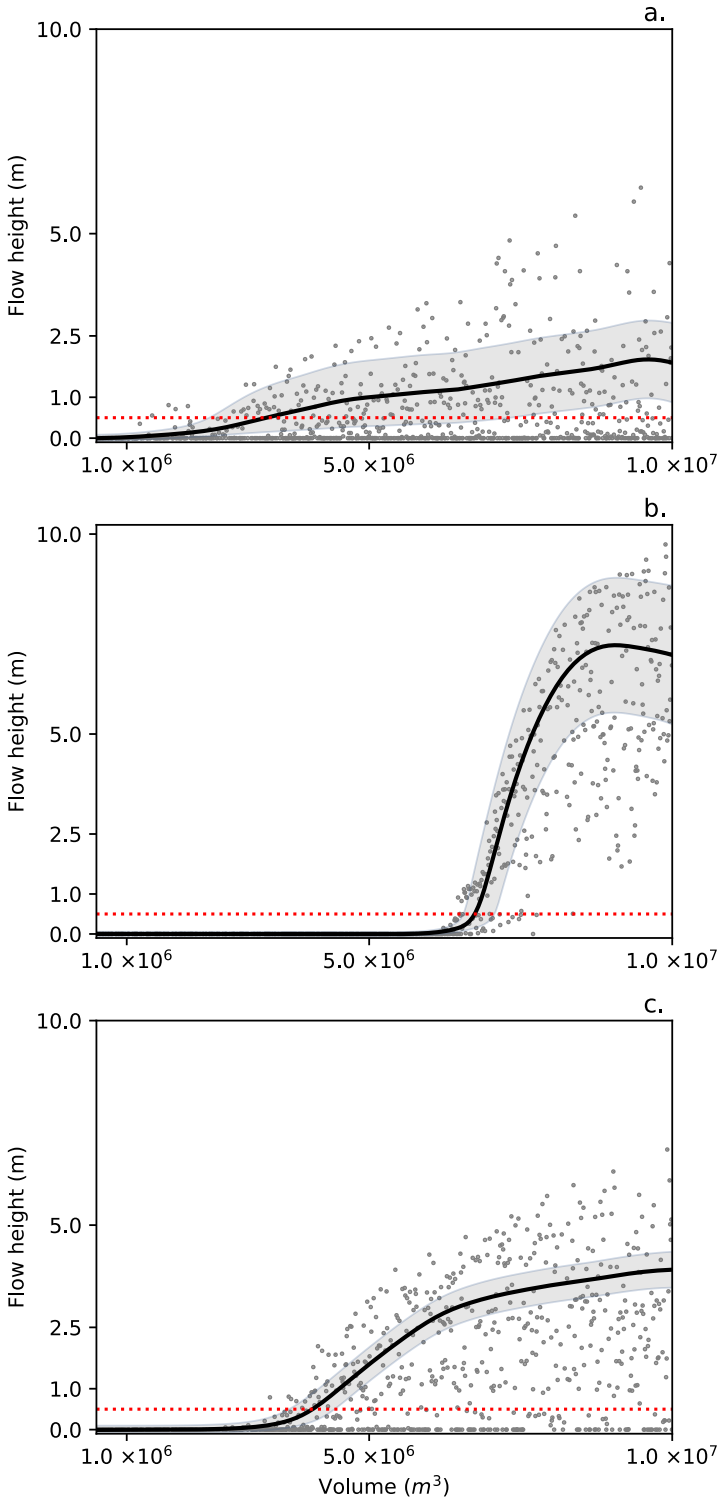

Figure 5. Emulator mean (black line) and 95% confidence interval (shaded) predictions for dome collapse flows in a similar configuration to the current (remnant) Taranaki dome at (a) Ahukawakawa, (b) Stony River, and (c) Kokowai Stream locations. Grey dots indicate simulated flow heights from all simulations.

Emulator slices can also be used to estimate impacts in new dome configurations (e.g. following explosive modification of summit). For example, Figure 6 shows an example of emulated flow heights for a dome collapse volume of 7.0×10^6 m^3 across the major axis orientation which can be used to evaluate directionality effects of dome collapse flows. A circular shape would indicate the dome major axis has no effect on maximum flow height (i.e. no directionality effects). Figure 6 shows clear variations in flow height with major axis angle, with a preference for larger flow heights when the dome is oriented towards the location.

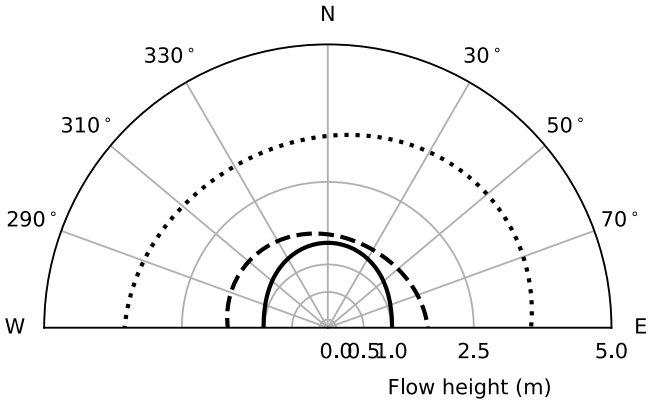

Figure 6. Emulator mean predictions for dome collapse flow volumes of 7.0×10^6 m^3 with a similar configuration to the current (remnant) Taranaki dome and varied major axis orientation at Ahukawakawa (solid line), Stony River (dashed line), and Kokowai Stream (dotted line) locations.

4 Application to dome collapse hazard assessment

Referring to Figure 1, probabilistic hazard assessment requires both an easily sampled surrogate (the emulator) and a source model quantifying the probability of the input space. The exceedance probability of the hazard (flow height) can then be calculated using Monte Carlo samples of the source distributions to calculate flow height in the emulator (i.e. similar to Bebbington et al. 2008). With the emulator built (see previous), and uniform distributions assumed the dome orientation and location (N, E, θ) due to a lack of prior information, a frequency-volume distribution is required to define the hazard.

Figure 5 suggests dome collapse volumes need to be greater than the current remnant dome volume (~~1.5 x 10^6 m^3) to cause flow heights greater than 0.5 m. Dome collapses of this magnitude have occurred at Taranaki (the most recent summit dome volume was estimated by Platz et al. (2012) to be ~5.9 x 10^6 m^3 in volume before collapse). However, an episode of significant dome growth is required to generate such conditions. Therefore, the likelihood of block-and-ash flows affecting the locations of interest is limited by the occurrence of a sufficient dome growth episode.

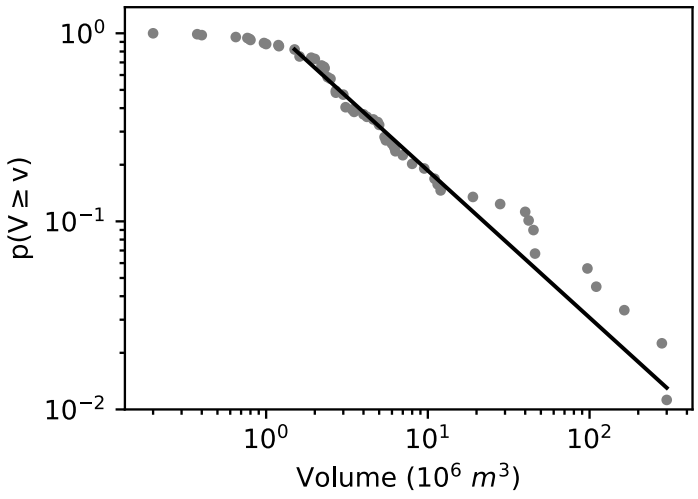

Figure 7. Log-log scale plot of proportion of dome collapse flow volumes exceeding volume *V*. Dots are empirical data from Harnett et al. (2019), black line is best fit power-law (α≈1.78) with a minimum volume of 1.5 × 10^6 m^3.

As there is no direct evidence of dome growth and collapse at Mt. Taranaki, we use the '*DomeHaz*' global dome growth dataset and analysis of Ogburn et al. (2015) to identify pathways to dome growth episodes capable of generating hazardous flows. The Ogburn et al. (2015) analysis notes it is most common to have an explosive eruption before dome growth episodes. They posit that large explosive eruptions may be necessary before dome growth episodes to remove high viscosity (i.e. cold rock) magma and lava from the conduit and enable extrusion of large magma volumes. This hypothesis is also supported by Platz (2007), using evidence from the most recent (Maero) eruptive period of Mt. Taranaki. Assuming an explosive eruption is required to precede a new episode of dome growth capable of producing hazardous

block-and-ash flows, and using the minimum dome extrusion rate (6.0 m^3s^{-1}) for the latest dome growth episode (Pyramid, Platz 2007); the probability tree of Ogburn et al. (2015) suggests there is a 0.73 probability of a dome growth episode, if an eruption occurs. This probability (0.73) relates to the chance of a dome growth episode following an eruption. As most lava domes do not collapse completely (see e.g. Ogburn and Calder 2017; Platz et al. 2007), instead releasing 50% to 80% of their total dome volume, the probability of dome collapse volumes, conditional on a sufficient growth episode needs to be calculated. A power-law distribution ($p(x) \propto x^{-\alpha}$) was used to fit andesitic dome collapse volumes in the Global Archive of Dome Instabilities database (Harnett et al. 2019). The frequency-volume plot in Figure 7 shows the data are well-fit by the distribution between 1.5 x 10^6 and 10^7 m^3 with an α of 1.78.

Figure 8 shows dome collapse flow height exceedance probability, conditional on a new dome growth episode, for all locations calculated from 10,000 dome configurations and 10 draws of the emulator posterior. Smaller flows (heights < 1.0 m) are more likely at the Kokowai (dotted line) and Ahukawakawa (solid line) locations, potentially due to their proximity to the dome.

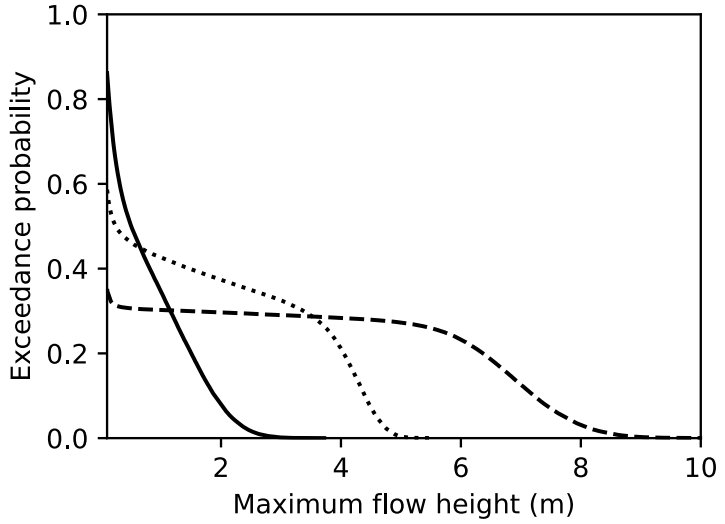

Figure 8. Flow height exceedance probabilities for Ahukawakawa (black line), Stony River (dashed line), and Kokowai Stream (dotted line) locations. Probabilities are conditional on a new dome growth episode following an eruption (p = 0.73).

However, larger flows (> 4 m) are much more likely to occur in the Stony River, as a result of the topographic controls directing most mass flows along this catchment (Procter et al. 2010).

5 Discussion

The use of surrogates for computationally expensive simulations have a dual purpose in the probabilistic hazard methodology used here. First, the surrogate emulator can be rapidly sampled, alleviating the computational burden when sampling using Monte-Carlo estimation. The 300,000 (3 × 100,000) samples in this example (Figure 8) took only 7 minutes on a desktop computer using an unoptimized sampling algorithm. In contrast, a single simulation using Titan2D can take up to 6 hours in a high-performance, parallel computing environment.

The emulator also provides a continuous approximation of hazard across the input space, as opposed to a discrete set of simulations. This continuous approximation supports easier updating of the hazard estimate in response to changes in source probabilities. For example, if the location and orientation of new dome growth is known, the exceedance probabilities can be updated in minutes through Monte-Carlo sampling of the emulator, rather than requiring a new set of computationally expensive simulations. Used as described here, emulation provides a preferable solution to quantifying mass flow hazard in a probabilistic manner over 'brute force' applications running many thousands of simulations, even if computational cost is not a factor for consideration.

These benefits can be limited by the simulation and simulator design space. If the simulation is inadequate or approximations are required outside the design space, the emulator will provide a bad fit. Simulator (model choice) inaccuracies can be simply addressed through informed model choice and calibration or model averaging (Akhavan-Safaei et al. 2017) as simulators are treated as a 'black box' by the emulator, only relying on the input (χ) and output (y) vectors. Definition of the input space can cause issues in emulation, as the space needs to

be broad enough to cover all eventualities, while narrow enough to provide an adequate density of data for the emulator. In particular, non-stationarity is a difficult issue for mass flow emulation (Rutarindwa et al. 2019; Spiller et al. 2014). Output warping (Snelson et al. 2004) performed satisfactorily for this application (see cross-validation results in Figure 4) and appears simpler to apply than previously suggested sub-emulators.

6 Conclusion

This methodology for probabilistic hazard assessment using deterministic simulations used Gaussian Process emulators as a statistical surrogate for simulation results. The emulator created a linear mapping between dome collapse flow inputs (volume, location, orientation) and simulated maximum flow heights, with non-stationarity in outputs addressed using a warping function fit with the emulator. Emulators created at three locations for dome collapse flow simulations at Taranaki volcano, New Zealand were found to approximate the simulations well (>90% within 2 standard deviations using leave-one-out cross validation). These created emulators act as a fast engine for probabilistic volcanic hazard assessment, enabling the use of standard Monte Carlo methods to estimate dome collapse flow hazard. This method has been successfully applied to a probabilistic estimation of hazard at key locations within the Egmont National Park at Taranaki, the application of which will be explored in future work. This methodology incorporating deterministic simulations and gaussian process emulators is not specific to dome collapse flows, and can be readily applied to other volcanic hazards and geo-hazards in general, provided a well-defined input space.

Computer Code Availability

The open-source python code for the Probabilistic Surrogate, including sample data, is available from https://github.com/stuartmead/probablisticsurrogate. Modified Titan2D simulator source code used to create the source data is available in the Zenodo repository https://doi.org/10.5281/zeondo.153.993.

Acknowledgements

The authors acknowledge the use of the New Zealand eScience Infrastructure (NeSI) high performance computing facilities as part of this research. We acknowledge the funding support of the MBIE Endeavour Programme 'Transitioning Taranaki to a Volcanic Future' UOAX1913.

References

Aguilera E, Pareschi MT, Rosi M, Zanchetta G (2004) Risk from Lahars in the Northern Valleys of Cotopaxi Volcano (Ecuador) Natural Hazards 33:161-189 doi:10.1023/B:NHAZ.0000037037.03155.23

Akhavan-Safaei A, Bevilacqua A, Patra A, Bursik M (2017) A Bayesian Framework for Rheology Model Combination and UQ in Simulation of Geophysical Mass Flows.

Alloway B, McComb P, Neall V, Vucetich C, Gibb J, Sherburn S, Stirling M (2005) Stratigraphy, age, and correlation of voluminous debris‐avalanche events from an ancestral Egmont Volcano: Implications for coastal plain construction and regional hazard assessment Journal of the Royal Society of New Zealand 35:229-267 doi:10.1080/03014223.2005.9517782

Bayarri MJ et al. (2009) Using Statistical and Computer Models to Quantify Volcanic Hazards Technometrics 51:402-413 doi:10.1198/TECH.2009.08018

Bebbington M, Cronin SJ, Chapman I, Turner MB (2008) Quantifying volcanic ash fall hazard to electricity infrastructure Journal of Volcanology and Geothermal Research 177:1055-1062 doi:10.1016/j.jvolgeores.2008.07.023

Bebbington MS (2014) Long-term forecasting of volcanic explosivity Geophysical Journal International 197:1500-1515 doi:10.1093/gji/ggu078

Bebbington MS, Jenkins SF (2019) Intra-eruption forecasting Bulletin of Volcanology 81:34 doi:10.1007/s00445-019-1294-9

Bebbington MS, Stirling MW, Cronin S, Wang T, Jolly G (2018) National-level long-term eruption forecasts by expert elicitation Bulletin of Volcanology 80:56 doi:10.1007/s00445-018-1230-4

Berger JO, De Oliveira V, Sansó B (2001) Objective Bayesian Analysis of Spatially Correlated Data Journal of the American Statistical Association 96:1361-1374 doi:10.1198/016214501753382282

Bevilacqua A et al. (2017) The Effects of Vent Location, Event Scale, and Time Forecasts on Pyroclastic Density Current Hazard Maps at Campi Flegrei Caldera (Italy) Frontiers in Earth Science 5 doi:10.3389/feart.2017.00072

Biass S, Bonadonna C, di Traglia F, Pistolesi M, Rosi M, Lestuzzi P (2016) Probabilistic evaluation of the physical impact of future tephra fallout events for the Island of Vulcano, Italy Bulletin of Volcanology 78:37 doi:10.1007/s00445-016-1028-1

Bonadonna C, Connor CB, Houghton BF, Connor L, Byrne M, Laing A, Hincks TK (2005) Probabilistic modeling of tephra dispersal: Hazard assessment of a multiphase rhyolitic eruption at Tarawera, New Zealand Journal of Geophysical Research: Solid Earth 110:n/a-n/a doi:10.1029/2003JB002896

Brown SK, Jenkins SF, Sparks RSJ, Odbert H, Auker MR (2017) Volcanic fatalities database: analysis of volcanic threat with distance and victim classification J Appl Volcanol 6:15 doi:10.1186/s13617-017-0067-4
Brown SK et al. (2015) Global volcanic hazard and risk. In: Vye-Brown C, Brown SK, Sparks S, Loughlin SC, Jenkins SF (eds) Global Volcanic Hazards and Risk. Cambridge University Press, Cambridge, pp 81-172. doi:DOI: 10.1017/CBO9781316276273.004
Calder E, Wagner K, Ogburn SE (2015) Volcanic hazard maps. In: Loughlin SC, Sparks RSJ, Brown SK, Jenkins SF, Vye-Brown C (eds) Global Volcanic Hazards and Risk. Cambridge University Press. doi:10.1017/CBO9781316276273.022
Carpignano A, Golia E, Di Mauro C, Bouchon S, Nordvik JP (2009) A methodological approach for the definition of multi‐risk maps at regional level: first application Journal of Risk Research 12:513-534 doi:10.1080/13669870903050269
Charbonnier S, Gertisser R (2009) Numerical simulations of block-and-ash flows using the Titan2D flow model: examples from the 2006 eruption of Merapi Volcano, Java, Indonesia Bulletin of Volcanology 71:953-959 doi:10.1007/s00445-009-0299-1
Connor C, Bebbington M, Marzocchi W (2015) Probabilistic Volcanic Hazard Assessment. In: Sigurdsson H (ed) The Encyclopedia of Volcanoes (Second Edition). Academic Press, Amsterdam, pp 897-910. doi:10.1016/B978-0-12-385938-9.00051-1
Cornell CA (1968) Engineering seismic risk analysis Bulletin of the Seismological Society of America 58:1583-1606
Dalbey K, Patra AK, Pitman EB, Bursik MI, Sheridan MF (2008) Input uncertainty propagation methods and hazard mapping of geophysical mass flows Journal of Geophysical Research: Solid Earth 113:n/a-n/a doi:10.1029/2006JB004471
Damaschke M, Cronin SJ, Bebbington MS (2018) A volcanic event forecasting model for multiple tephra records, demonstrated on Mt. Taranaki, New Zealand Bulletin of Volcanology 80:9 doi:10.1007/s00445-017-1184-y
Duvenaud D, Lloyd JR, Grosse R, Tenenbaum JB, Ghahramani Z Structure discovery in nonparametric regression through compositional kernel search. In: Proceedings of the 30th International Conference on International Conference on Machine Learning-Volume 28, 2013. JMLR. org, pp III-1166
Gramacy RB, Lee HKH (2008) Bayesian Treed Gaussian Process Models With an Application to Computer Modeling Journal of the American Statistical Association 103:1119-1130 doi:10.1198/016214508000000689
Gu M (2019) Jointly Robust Prior for Gaussian Stochastic Process in Emulation, Calibration and Variable Selection Bayesian Anal 14:857-885 doi:10.1214/18-BA1133
Gu M, Berger JO (2016) Parallel partial Gaussian process emulation for computer models with massive output Ann Appl Stat 10:1317-1347 doi:10.1214/16-AOAS934
Gu M, Wang X, Berger JO (2018) Robust Gaussian stochastic process emulation Ann Statist 46:3038-3066 doi:10.1214/17-AOS1648
Harnett CE, Thomas ME, Calder ES, Ebmeier SK, Telford A, Murphy W, Neuberg J (2019) Presentation and analysis of a worldwide database for lava dome collapse events: the Global Archive of Dome Instabilities (GLADIS) Bulletin of Volcanology 81:1-17
Hawker L, Rougier J, Neal J, Bates P, Archer L, Yamazaki D (2018) Implications of Simulating Global Digital Elevation Models for Flood Inundation Studies Water Resources Research 54:7910-7928 doi:10.1029/2018wr023279
Hill BE, Aspinall WP, Connor CB, Godoy AR, Komorowski JC, Nakada S (2009) Recommendations for assessing volcanic hazards at sites of nuclear installations. In: Connor CB, Connor LJ, Chapman NA (eds) Volcanic and Tectonic Hazard

Assessment for Nuclear Facilities. Cambridge University Press, Cambridge, pp 566-592. doi:DOI: 10.1017/CBO9780511635380.026
Hurst T, Smith W (2004) A Monte Carlo methodology for modelling ashfall hazards Journal of Volcanology and Geothermal Research 138:393-403 doi:10.1016/j.jvolgeores.2004.08.001
Hurst T, Smith W (2010) Volcanic ashfall in New Zealand – probabilistic hazard modelling for multiple sources New Zealand Journal of Geology and Geophysics 53:1-14 doi:10.1080/00288301003631129
Iverson RM, George DL (2014) A depth-averaged debris-flow model that includes the effects of evolving dilatancy. I. Physical basis vol 470. vol 2170. doi:10.1098/rspa.2013.0819
Jenkins S, Magill C, McAneney J, Blong R (2012) Regional ash fall hazard I: a probabilistic assessment methodology Bulletin of Volcanology 74:1699-1712 doi:10.1007/s00445-012-0627-8
Jenkins SF, Magill CR, McAneney KJ (2007) Multi-stage volcanic events: A statistical investigation Journal of Volcanology and Geothermal Research 161:275-288 doi:10.1016/j.jvolgeores.2006.12.005
Kelfoun K (2017) A two-layer depth-averaged model for both the dilute and the concentrated parts of pyroclastic currents Journal of Geophysical Research: Solid Earth 122:4293-4311 doi:10.1002/2017JB014013
Kelfoun K, Gueugneau V, Komorowski J-C, Aisyah N, Cholik N, Merciecca C (2017) Simulation of block-and-ash flows and ash-cloud surges of the 2010 eruption of Merapi volcano with a two-layer model Journal of Geophysical Research: Solid Earth 122:4277-4292 doi:10.1002/2017JB013981
Kennedy MC, O'Hagan A (2001) Bayesian calibration of computer models Journal of the Royal Statistical Society: Series B (Statistical Methodology) 63:425-464 doi:10.1111/1467-9868.00294
Landcare Research NZ L (2002) NZDEM North Island 25 metre. doi:10.26060/6AS4-4Z82
Lerner GA, Cronin SJ, Bebbington MS, Platz T (2019) The characteristics of a multi-episode volcanic regime: the post-AD 960 Maero Eruptive Period of Mt. Taranaki (New Zealand) Bulletin of Volcanology 81:61 doi:10.1007/s00445-019-1327-4
Lloyd JR, Duvenaud D, Grosse R, Tenenbaum J, Ghahramani Z (2014) Automatic Construction and Natural-Language Description of Nonparametric Regression Models. 2014.
Magill C, Blong R (2005) Volcanic risk ranking for Auckland, New Zealand. I: Methodology and hazard investigation Bulletin of Volcanology 67:331-339 doi:10.1007/s00445-004-0374-6
Mahmood A, Wolpert R, Pitman E (2015) A Physics-Based Emulator for the Simulation of Geophysical Mass Flows SIAM/ASA Journal on Uncertainty Quantification 3:562-585 doi:10.1137/130909445
Marzocchi W, Garcia-Aristizabal A, Gasparini P, Mastellone ML, Di Ruocco A (2012) Basic principles of multi-risk assessment: a case study in Italy Natural Hazards 62:551-573 doi:10.1007/s11069-012-0092-x
Mead S, Magill C (2014) Determining change points in data completeness for the Holocene eruption record Bulletin of Volcanology 76:1-14 doi:10.1007/s00445-014-0874-y
Mead SR, Magill CR (2017) Probabilistic hazard modelling of rain-triggered lahars J Appl Volcanol 6:8 doi:10.1186/s13617-017-0060-y
Nadejda K, Anna S, Alexander G-A, Daniel M, Kevin F (2016) Multi-risk approach and urban resilience International Journal of Disaster Resilience in the Built Environment 7:114-132 doi:10.1108/IJDRBE-03-2015-0013

Neall V, Stewart R, Smith I (1986) History and petrology of the Taranaki volcanoes Royal Society of New Zealand Bulletin 23:251-263
Neall VE (1979) Geological Map of New Zealand: Sheets P19, P20, & P21: New Plymouth, Egmont, and Manaia. Department of Scientific and Industrial Research,
Ogburn SE, Calder ES (2017) The Relative Effectiveness of Empirical and Physical Models for Simulating the Dense Undercurrent of Pyroclastic Flows under Different Emplacement Conditions Frontiers in Earth Science 5 doi:10.3389/feart.2017.00083
Ogburn SE, Loughlin SC, Calder ES (2015) The association of lava dome growth with major explosive activity (VEI ≥ 4): DomeHaz, a global dataset Bulletin of Volcanology 77:40 doi:10.1007/s00445-015-0919-x
Paciorek CJ, Schervish MJ Nonstationary covariance functions for Gaussian process regression. In: Advances in neural information processing systems, 2004. pp 273-280
Pareschi M (2000) GlS and volcanic risk assessment Natural Hazards 21:361-379
Patra AK et al. (2005) Parallel adaptive numerical simulation of dry avalanches over natural terrain Journal of Volcanology and Geothermal Research 139:1-21 doi:10.1016/j.jvolgeores.2004.06.014
Pitman EB, Nichita CC, Patra A, Bauer A, Sheridan M, Bursik M (2003) Computing granular avalanches and landslides Phys Fluids 15:3638-3646 doi:10.1063/1.1614253
Platz T (2007) Understanding aspects of andesitic dome-forming eruptions through the last 1000 yrs of volcanism at Mt. Taranaki, New Zealand : a dissertation presented in partial fulfilment of the requirements for the degree of Doctor of Philosophy in Earth Science, Massey University, Palmerston North, New Zealand. Doctoral, Massey University
Platz T, Cronin SJ, Cashman KV, Stewart RB, Smith IEM (2007) Transition from effusive to explosive phases in andesite eruptions — A case-study from the AD1655 eruption of Mt. Taranaki, New Zealand Journal of Volcanology and Geothermal Research 161:15-34 doi:10.1016/j.jvolgeores.2006.11.005
Platz T, Cronin SJ, Procter JN, Neall VE, Foley SF (2012) Non-explosive, dome-forming eruptions at Mt. Taranaki, New Zealand Geomorphology 136:15-30 doi:10.1016/j.geomorph.2011.06.016
Procter J, Cronin S, Platz T, Patra A, Dalbey K, Sheridan M, Neall V (2010) Mapping block-and-ash flow hazards based on Titan 2D simulations: a case study from Mt. Taranaki, NZ Natural Hazards 53:483-501 doi:10.1007/s11069-009-9440-x
Procter JN, Zernack AV, Cronin SJ (2021) Computer Simulation of a Volcanic Debris Avalanche from Mt. Taranaki, New Zealand. In: Roverato M, Dufresne A, Procter J (eds) Volcanic Debris Avalanches: From Collapse to Hazard. Springer International Publishing, Cham, pp 281-310. doi:10.1007/978-3-030-57411-6_11
Pudasaini SP (2012) A general two-phase debris flow model Journal of Geophysical Research: Earth Surface 117 doi:10.1029/2011JF002186
Pudasaini SP, Miller SA (2013) The hypermobility of huge landslides and avalanches Engineering Geology 157:124-132 doi:10.1016/j.enggeo.2013.01.012
Rasmussen CaW, CKI (2006) Gaussian Processes for Machine Learning. Adaptive Computation and Machine Learning. The MIT Press, Cambridge, Massachusetts
Rhoades DA, Dowrick DJ, Wilson CJN (2002) Volcanic Hazard in New Zealand: Scaling and Attenuation Relations for Tephra fall deposits from Taupo Volcano Natural Hazards 26:147-174 doi:10.1023/A:1015608732356
Rutarindwa R, Spiller ET, Bevilacqua A, Bursik MI, Patra AK (2019) Dynamic Probabilistic Hazard Mapping in the Long Valley Volcanic Region CA: Integrating Vent Opening Maps and Statistical Surrogates of Physical Models of Pyroclastic Density Currents

Journal of Geophysical Research: Solid Earth 124:9600-9621 doi:10.1029/2019JB017352
Sacks J, Welch WJ, Mitchell TJ, Wynn HP (1989) Design and Analysis of Computer Experiments Statistical Science 4:409-423
Sandri L, Jolly G, Lindsay J, Howe T, Marzocchi W (2012) Combining long- and short-term probabilistic volcanic hazard assessment with cost-benefit analysis to support decision making in a volcanic crisis from the Auckland Volcanic Field, New Zealand Bulletin of Volcanology 74:705-723 doi:10.1007/s00445-011-0556-y
Santner TJ, Williams BJ, Notz W, Williams BJ (2003) The design and analysis of computer experiments vol 1. Springer,
Sheridan MF, Stinton AJ, Patra A, Pitman EB, Bauer A, Nichita CC (2005) Evaluating Titan2D mass-flow model using the 1963 Little Tahoma Peak avalanches, Mount Rainier, Washington Journal of Volcanology and Geothermal Research 139:89-102 doi:10.1016/j.jvolgeores.2004.06.011
Snelson E, Ghahramani Z, Rasmussen CE Warped gaussian processes. In: Advances in neural information processing systems, 2004. pp 337-344
Snoek J, Swersky K, Zemel R, Adams R Input warping for Bayesian optimization of non-stationary functions. In: International Conference on Machine Learning, 2014. pp 1674-1682
Spiller E, Bayarri M, Berger J, Calder E, Patra A, Pitman E, Wolpert R (2014) Automating Emulator Construction for Geophysical Hazard Maps SIAM/ASA Journal on Uncertainty Quantification 2:126-152 doi:10.1137/120899285
Stefanescu ER et al. (2012) Digital elevation model uncertainty and hazard analysis using a geophysical flow model Proceedings of the Royal Society A: Mathematical, Physical and Engineering Science 468:1543
Stirling M et al. (2017) Conceptual Development of a National Volcanic Hazard Model for New Zealand Frontiers in Earth Science 5 doi:10.3389/feart.2017.00051
Stirling M, Wilson C (2002) Development of a volcanic hazard model for New Zealand: first approaches from the methods of probabilistic seismic hazard analysis Bulletin of the New Zealand Society for Earthquake Engineering 35:266-277
Torres-Orozco R, Cronin SJ, Damaschke M, Pardo N (2017) Diverse dynamics of Holocene mafic-intermediate Plinian eruptions at Mt. Taranaki (Egmont), New Zealand Bulletin of Volcanology 79:76 doi:10.1007/s00445-017-1162-4
Torres-Orozco R, Cronin SJ, Pardo N, Palmer AS (2016) New insights into Holocene eruption episodes from proximal deposit sequences at Mt. Taranaki (Egmont), New Zealand Bulletin of Volcanology 79:3 doi:10.1007/s00445-016-1085-5
Vehtari A, Mononen T, Tolvanen V, Sivula T, Winther O (2016) Bayesian leave-one-out cross-validation approximations for Gaussian latent variable models J Mach Learn Res 17:3581–3618
Wang T, Bebbington M (2012) Estimating the likelihood of an eruption from a volcano with missing onsets in its record Journal of Volcanology and Geothermal Research 243–244:14-23 doi:10.1016/j.jvolgeores.2012.06.032
Wolpert RL, Spiller ET, Calder ES (2018) Dynamic Statistical Models for Pyroclastic Density Current Generation at Soufrière Hills Volcano Frontiers in Earth Science 6 doi:10.3389/feart.2018.00055
Zernack AV (2008) A sedimentological and geochemical approach to understanding cycles of stratovolcano growth and collapse at Mt Taranaki, New Zealand. Massey University
Zernack AV, Procter JN (2021) Cyclic Growth and Destruction of Volcanoes. In: Roverato M, Dufresne A, Procter J (eds) Volcanic Debris Avalanches: From Collapse to

Hazard. Springer International Publishing, Cham, pp 311-355. doi:10.1007/978-3-030-57411-6_12